International Journal of Automotive Technology, Vol. 20, No. 4, pp. 679–691 (2019)
DOI 10.1007/s12239–019–0064–1

pISSN 1229–9138/ eISSN 1976–3832

LPV/H_∞ CONTROLLER DESIGN FOR PATH TRACKING OF AUTONOMOUS GROUND VEHICLES THROUGH FOUR-WHEEL STEERING AND DIRECT YAW-MOMENT CONTROL

Peng Hang[1, 2], Xinbo Chen[1, 2)*] and Fengmei Luo[1)]

[1)]School of Automotive Studies, Tongji University, Shanghai 201804, China
[2)]Clean Energy Automotive Engineering Center, Tongji University, Shanghai 201804, China

(Received 2 January 2018; Revised 19 October 2018; Accepted 19 December 2018)

ABSTRACT–This paper focuses on the path-tracking controller design for autonomous ground vehicles (AGVs) using four-wheel steering (4WS) and direct yaw-moment control (DYC) systems. In order to deal with the parametric uncertainties, a linear parameter-varying (LPV) H_∞ controller is designed as the high-level controller to generate the front and rear wheel steering angles and external yaw moment based on linear matrix inequality (LMI) approach. The lower-level controller is designed for torque allocation between the left and right side wheels to yield the desired total longitudinal force and external yaw moment utilizing weighted least square (WLS) allocation algorithm. To test the performance of the proposed path-tracking controller, numerical simulations are carried out based on a high-fidelity and full-vehicle model constructed in CarSim. Simulation results show that the LPV/H_∞ controller has better path-tracking performance than the fixed gain H_∞ controller. To show the superiority of 4WS+DYC control system, the contrast simulation is performed based on LPV/H_∞ controller. Simulation results indicate that 4WS+DYC control system has better path-tracking performance and handling stability than active front steering (AFS), AFS+DYC and 4WS control systems.

KEY WORDS : Path tracking, Linear parameter-varying, Robust control, Four-wheel steering, Direct yaw-moment control

1. INTRODUCTION

In recent years, a large number of studies about intelligent transport systems (ITSs) have been carried out to address various traffic problems such as congestion and accidents (Backfrieder *et al*., 2017; Zhou *et al*., 2017). Especially, automatic driving technology has become a very active research field of ITSs. Path-tracking control of autonomous ground vehicles (AGVs) is the fundamental research and significant part of automatic driving technology. The primary task of path-tracking control can be described as making the AGV to follow a target path automatically. The designed path-tracking controller aims to minimize the lateral offset and heading error between the vehicle and target path while maintaining the stability (Hang *et al*., 2017a).

Numerous control algorithms and strategies have been applied to solving the problem of path tracking, such as adaptive neural control (Wang *et al*., 2015a), output constraint control (Hu *et al*., 2016), genetic algorithm (Guo *et al*., 2012), fuzzy control (El Hajjaji and Bentalba, 2003), sliding mode control (SMC) (Janbakhsh *et al*., 2013; Tchenderli-Braham *et al*., 2015), model predictive control (MPC) (Kim *et al*., 2014; Yu *et al*., 2015), optimal control (Goodarzi *et al*., 2008; Hu *et al*., 2015), robust control (You and Jeong, 2002), etc. However, most of the path-tracking controllers are designed for the conventional internal combustion engine drive vehicles (ICVs) with active front steering (AFS) systems. Compared with ICVs, electric vehicles (EVs) have several advantages in the fields of emission reduction, energy efficiency, performance benefits, and so on (Wang *et al*., 2011). Among all the kinds of EVs, the four-wheel independent steering (4WIS) and four-wheel independent drive (4WID) EV is more suitable for an AGV, in which the steering angle and drive torque of each wheel both can be controlled independently thanks to four steering motors and four drive motors (Chen *et al*., 2006; Lam *et al*., 2010; Zong *et al*., 2011). For this reason, the 4WIS-4WID EV can achieve better dynamic performances by four-wheel steering (4WS) and yaw-moment control (DYC) systems than conventional ICVs. At low speed, 4WS system can help the vehicle reduce turning radius so as to improve maneuverability by anti-phase steering of the front and rear wheels. Moreover, 4WS and DYC systems can help the vehicle realize zero sideslip angle and desired yaw rate to improve handling stability by in-phase steering of the front and rear wheels at high speed (Hang *et al*., 2017b).

Since the control degrees of freedom (DoF) of the 4WIS-4WID EV are much more than that of the

**Corresponding author*. e-mail: chenxinbo@tongji.edu.cn

conventional AFS ICVs. Accordingly, the path-tracking problem of 4WIS-4WID EV is more complex and the control strategies are still relatively limited (Hiraoka *et al*., 2009). Nevertheless, numerous researchers have done a lot of studies on the path-tracking control of AGVs using 4WS or AFS+DYC systems. A path-tracking controller was proposed for 4WS vehicles based on optimal control by Mashadi *et al*. (2011), the designed controller works well and shows great path-tracking potential of 4WS system. However, the optimal controller is designed for nominal vehicle model without considering the parametric uncertainties and external disturbances. In other word, the designed optimal controller does not have robustness. To make the path-tracking controller obtain robustness against parametric uncertainties and external disturbances, an automatic path-tracking controller was designed for of a 4WS vehicle using SMC theory by Hiraoka *et al*. (2009), which has a more precise path-tracking capability than that of AFS path-tracking controller and has robust capability against system uncertainties. Based on MPC theory, an output-feedback path-tracking controller for 4WS AGVs was proposed by Yakub and Mori (2015) and Yakub *et al*. (2016), and the controller is capable of maintaining vehicle stability along the desired path and eliminating the crosswind effect. Except for 4WS system, DYC is another effective way combined with AFS to improve the vehicle dynamic performances (Xiong *et al*., 2012; Zhang *et al*., 2014; Wang *et al*., 2015b; Yin *et al*., 2015; Zhao *et al*., 2015; Kobayashi *et al*., 2017). Especially for the 4WID EV with four in-wheel motors, the drive and brake torque of each in-wheel motor can be controlled independently, which is quite easy to realize DYC. A MPC path-tracking controller was studied for a 4WIS-4WID EV using 4WS+DYC system by Hang *et al*. (2017c), the controller shows good path-tracking performance and strong robust performance against parametric perturbations. An integrated 4WS+DYC robust controller for AGVs was designed in by Mashadi *et al*. (2015) utilizing μ synthesis approach, which has a profound ability to make the vehicle track the desired path in the presence of parametric uncertainties. To this end, both 4WS and DYC are proposed for path-tracking controller design of a 4WIS-4WID EV in this paper.

The rest of the paper is organized as follows. The path-tracking model of the 4WIS-4WID EV and its polytopic model considering parametric uncertainties are presented in Section 2. Section 3 deals with the path-tracking controller design of the 4WIS-4WID EV, including the higher-level LPV/H_∞ controller and the lower-level control allocation algorithm. The performance of the designed path-tracking controller is verified in Section 4 based on simulation analysis with a high-fidelity and full-vehicle model via CarSim-Simulink platform. Finally, Section 5 presents concluding remarks and describes areas for future work.

2. SYSTEM MODELING

2.1. Path-tracking Model

To simplify the dynamic model of the 4WIS-4WID EV for controller design, without considering the pitch and roll motions, only the planar motion is taken into account. As a result, the simplified vehicle model with 2 DoF is illustrated in Figure 1. Moreover, the two front wheels and two rear wheels are assumed to be lumped together at the centers of front and rear axles, respectively. The four-wheel vehicle model is simplified as a single track model, and its handling dynamic model can be described by

$$\begin{aligned} \dot{v}_{\mathrm{y}} &= \frac{1}{m}(F_{\mathrm{yf}}\cos\delta_{\mathrm{f}} + F_{\mathrm{yr}}\cos\delta_{\mathrm{r}}) - v_{\mathrm{x}} r \\ \dot{r} &= \frac{1}{I_{\mathrm{z}}}(l_{\mathrm{f}}F_{\mathrm{yf}}\cos\delta_{\mathrm{f}} - l_{\mathrm{r}}F_{\mathrm{yr}}\cos\delta_{\mathrm{r}}) + \frac{1}{I_{\mathrm{z}}}\Delta M_{\mathrm{z}} \end{aligned} \tag{1}$$

where v_{x} and v_{y} are the vehicle longitudinal and lateral velocities, respectively. r is the yaw rate. m and I_{z} are the vehicle mass and yaw inertia. F_{yf} and F_{yr} are the front and rear tire lateral forces. δ_{f} and δ_{r} are the front and rear wheel steering angles. l_{f} and l_{r} are the front and rear wheel bases. ΔM_{z} is the external yaw moment generated by the longitudinal tire force difference between the left and right side wheels, which can be expressed as

$$\Delta M_{\mathrm{z}} = \frac{B}{2}(-F_{\mathrm{xfl}} + F_{\mathrm{xfr}} - F_{\mathrm{xrl}} + F_{\mathrm{xrr}}) \tag{2}$$

where B denotes the vehicle track, F_{xi} (i = *fl*, *fr*, *rl*, *rr*) denotes the longitudinal force of each tire.

Providing that the tire slip angle is much small at high vehicle speed, the relationship between the lateral tire force and tire slip angle can be demonstrated as linear relationship, which can be written as

$$F_{\mathrm{yf}} = -k_{\mathrm{f}}\alpha_{\mathrm{f}}, \qquad F_{\mathrm{yr}} = -k_{\mathrm{r}}\alpha_{\mathrm{r}} \tag{3}$$

where k_{f} and k_{r} are the cornering stiffness of the front and rear tires, respectively. α_{f} and α_{r} are the front and rear tire slip angles, which are defined as

$$\alpha_{\mathrm{f}} = \frac{v_{\mathrm{y}} + l_{\mathrm{f}} r}{v_{\mathrm{x}}} - \delta_{\mathrm{f}}, \qquad \alpha_{\mathrm{r}} = \frac{v_{\mathrm{y}} - l_{\mathrm{r}} r}{v_{\mathrm{x}}} - \delta_{\mathrm{r}} \tag{4}$$

Assuming that the front and rear wheel steering angles are small at high vehicle speed, approximately, $\cos\delta_{\mathrm{f}} \approx \cos\delta_{\mathrm{r}} \approx 1$ in Equation (1). Based on the Equations (3) and (4), the vehicle model described by Equation (1) can be simplified as a linear dynamic equation, which is derived as

$$\begin{aligned} \dot{v}_{\mathrm{y}} &= -\frac{k_{\mathrm{f}} + k_{\mathrm{r}}}{m v_{\mathrm{x}}} v_{\mathrm{y}} - \left(\frac{l_{\mathrm{f}}k_{\mathrm{f}} - l_{\mathrm{r}}k_{\mathrm{r}}}{m v_{\mathrm{x}}} + v_{\mathrm{x}}\right) r + \frac{k_{\mathrm{f}}}{m}\delta_{\mathrm{f}} + \frac{k_{\mathrm{r}}}{m}\delta_{\mathrm{r}} \\ \dot{r} &= -\frac{l_{\mathrm{f}}k_{\mathrm{f}} - l_{\mathrm{r}}k_{\mathrm{r}}}{I_{\mathrm{z}} v_{\mathrm{x}}} v_{\mathrm{y}} - \frac{l_{\mathrm{f}}^2 k_{\mathrm{f}} + l_{\mathrm{r}}^2 k_{\mathrm{r}}}{I_{\mathrm{z}} v_{\mathrm{x}}} r + \frac{l_{\mathrm{f}}k_{\mathrm{f}}}{I_{\mathrm{z}}}\delta_{\mathrm{f}} - \frac{l_{\mathrm{r}}k_{\mathrm{r}}}{I_{\mathrm{z}}}\delta_{\mathrm{r}} + \frac{\Delta M_{\mathrm{z}}}{I_{\mathrm{z}}} \end{aligned} \tag{5}$$

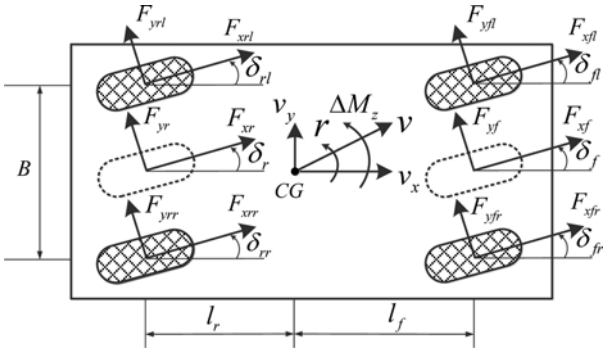

Figure 1. Planar motion model of 4WIS-4WID EV.

For path-tracking controller design, the path-tracking model of the 4WIS and 4WID EV is illustrated in Figure 2 utilizing the single track model. Three kinds of coordinate frame are adopted in Figure 2. The *xy* body coordinate frame denotes the vehicle direction on its actual path, $x_d y_d$ coordinate frame denotes the vehicle direction on its target path, and *XY* coordinate frame is the geodetic coordinate system. To make the vehicle track the target path precisely, the path-tracking problem is equivalent to minimize the yaw angle error $\Delta\varphi$ and the lateral position error Δy in this paper.

The yaw angle error is defined as the difference between the actual yaw angle φ and the target yaw angle φ_d, which is written as

$$\Delta\varphi = \varphi - \varphi_d \tag{6}$$

Taking a derivative with respect to time on the both sides of Equation (6) yields

$$\Delta\dot{\varphi} = \dot{\varphi} - \dot{\varphi}_d = r - \frac{v_x}{\rho} \tag{7}$$

where ρ denotes the curvature radius of the target path.

Additionally, the lateral position error Δy is defined as the vertical distance from the target path point *P* to *x* axis, and its derivative is derived as

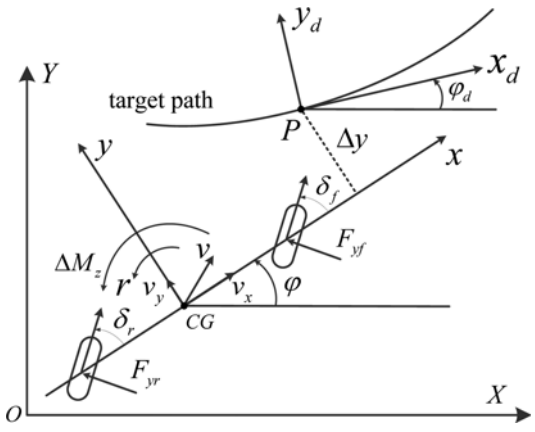

Figure 2. Single track model for path tracking.

$$\Delta\dot{y} = v_y + v_x\Delta\varphi \tag{8}$$

Based on Equations (5), (7) and (8), the path-tracking model can be rewritten as

$$\dot{x}_c = A_c x_c + B_{c1} w + B_{c2} u \tag{9}$$

where $x_c = \begin{bmatrix} v_y & r & \Delta y & \Delta\varphi \end{bmatrix}^T$, $w = \dfrac{1}{\rho}$,

$u = \begin{bmatrix} \delta_f & \delta_r & \Delta M_z \end{bmatrix}^T$, $B_{c1} = \begin{bmatrix} 0 & 0 & 0 & -v_x \end{bmatrix}^T$,

$$A_c = \begin{bmatrix} -\dfrac{k_f + k_r}{m v_x} & \dfrac{-l_f k_f + l_r k_r}{m v_x} - v_x & 0 & 0 \\ \dfrac{-l_f k_f + l_r k_r}{I_z v_x} & -\dfrac{l_f^2 k_f + l_r^2 k_r}{I_z v_x} & 0 & 0 \\ 1 & 0 & 0 & v_x \\ 0 & 1 & 0 & 0 \end{bmatrix},$$

$$B_{c2} = \begin{bmatrix} \dfrac{k_f}{m} & \dfrac{k_r}{m} & 0 \\ \dfrac{l_f k_f}{I_z} & -\dfrac{l_r k_r}{I_z} & \dfrac{1}{I_z} \\ 0 & 0 & 0 \\ 0 & 0 & 0 \end{bmatrix}.$$

2.2. Polytopic Model

Since vehicle longitudinal velocity and tire cornering stiffness have significant impacts on the vehicle handling stability, to make the vehicle achieve better dynamic performance, they are viewed as time-varying but measurable or observable parameters for linear parameter-varying (LPV) system construction. Considering that tire cornering stiffness is mainly affected by the road friction coefficient, the uncertainty of tire cornering stiffness can be converted into that of road friction coefficient. Therefore, the actual cornering stiffness of the front and rear tires can be expressed as $k_f = \mu k_{f0}$ and $k_r = \mu k_{r0}$, where μ denotes the road friction coefficient and k_{f0} and k_{r0} denote the nominal cornering stiffness of the front and rear tires. Therefore, the auxiliary time-varying parameters are chosen as $\theta_1 = \mu/v_x$, $\theta_2 = v_x$ and $\theta_3 = \mu$. Denoting parameter-varying vector $\Theta = [\theta_1\ \theta_2\ \theta_3]^T$, the LPV system for controller design can be described as

$$\begin{aligned} \dot{x}_c &= A_c(\Theta)x_c + B_{c1}(\Theta)w + B_{c2}(\Theta)u \\ y &= C_c x_c + D_{c1} w + D_{c2} u \end{aligned} \tag{10}$$

where

$$A_c(\Theta) = \begin{bmatrix} -\dfrac{k_{f0} + k_{r0}}{m}\theta_1 & \dfrac{-l_f k_{f0} + l_r k_{r0}}{m}\theta_1 - \theta_2 & 0 & 0 \\ \dfrac{-l_f k_{f0} + l_r k_{r0}}{I_z}\theta_1 & -\dfrac{l_f^2 k_{f0} + l_r^2 k_{r0}}{I_z}\theta_1 & 0 & 0 \\ 1 & 0 & 0 & \theta_2 \\ 0 & 1 & 0 & 0 \end{bmatrix},$$

$$B_{c1}(\Theta)=\begin{bmatrix}0\\0\\0\\-\theta_2\end{bmatrix},\quad B_{c2}(\Theta)=\begin{bmatrix}\frac{k_{f0}}{m}\theta_3 & \frac{k_{r0}}{m}\theta_3 & 0\\ \frac{l_f k_{f0}}{I_z}\theta_3 & -\frac{l_r k_{r0}}{I_z}\theta_3 & \frac{1}{I_z}\\ 0 & 0 & 0\\ 0 & 0 & 0\end{bmatrix},$$

$$C_c=\begin{bmatrix}0&0&1&0\\0&0&0&1\end{bmatrix},\quad D_{c1}=[0]_{2\times1},\quad D_{c2}=[0]_{2\times3}.$$

Furthermore, the affine models of the matrices $A_c(\Theta)$, $B_{c1}(\Theta)$ and $B_{c2}(\Theta)$ can be expressed as

$$\begin{aligned}A_c(\Theta)&=A_{c0}+\sum_{i=1}^{3}\theta_i A_{ci}\\ B_{c1}(\Theta)&=B_{c10}+\sum_{i=1}^{3}\theta_i B_{c1i}\\ B_{c2}(\Theta)&=B_{c20}+\sum_{i=1}^{3}\theta_i B_{c2i}\end{aligned}\tag{11}$$

where

$$A_{c0}=\begin{bmatrix}0&0&0&0\\0&0&0&0\\1&0&0&0\\0&1&0&0\end{bmatrix},\quad A_{c2}=\begin{bmatrix}0&-1&0&0\\0&0&0&0\\0&0&0&1\\0&0&0&0\end{bmatrix},$$

$$A_{c1}=\begin{bmatrix}-\frac{k_{f0}+k_{r0}}{m} & \frac{-l_f k_{f0}+l_r k_{r0}}{m} & 0&0\\ \frac{-l_f k_{f0}+l_r k_{r0}}{I_z} & -\frac{l_f^2 k_{f0}+l_r^2 k_{r0}}{I_z} & 0&0\\ 0&0&0&0\\0&0&0&0\end{bmatrix},$$

$$A_{c3}=[0]_{4\times4},\quad B_{c10}=[0]_{4\times1},\quad B_{c11}=[0]_{4\times1},\quad B_{c21}=[0]_{4\times3},$$

$$B_{c12}=\begin{bmatrix}0\\0\\0\\-1\end{bmatrix},\quad B_{c13}=[0]_{4\times1},\quad B_{c20}=\begin{bmatrix}0&0&0\\0&0&\frac{1}{I_z}\\0&0&0\\0&0&0\end{bmatrix},$$

$$B_{c22}=[0]_{4\times3},\quad B_{c23}=\begin{bmatrix}\frac{k_{f0}}{m}&\frac{k_{r0}}{m}&0\\ \frac{l_f k_{f0}}{I_z}&-\frac{l_r k_{r0}}{I_z}&0\\0&0&0\\0&0&0\end{bmatrix}.$$

Since $\theta_i\in\left[\theta_i^{\min},\ \theta_i^{\max}\right]$ (i = 1, 2, 3), parameter-varying vector Θ has eight kinds of combinations as follows.

$$\Theta_1=\left[\theta_1^{\max}\quad\theta_2^{\max}\quad\theta_3^{\max}\right]^{\mathrm{T}},\ \Theta_2=\left[\theta_1^{\max}\quad\theta_2^{\max}\quad\theta_3^{\min}\right]^{\mathrm{T}},$$

$$\Theta_3=\left[\theta_1^{\max}\quad\theta_2^{\min}\quad\theta_3^{\max}\right]^{\mathrm{T}},\ \Theta_4=\left[\theta_1^{\min}\quad\theta_2^{\max}\quad\theta_3^{\max}\right]^{\mathrm{T}},$$

$$\Theta_5=\left[\theta_1^{\max}\quad\theta_2^{\min}\quad\theta_3^{\min}\right]^{\mathrm{T}},\ \Theta_6=\left[\theta_1^{\min}\quad\theta_2^{\max}\quad\theta_3^{\min}\right]^{\mathrm{T}},$$

$$\Theta_7=\left[\theta_1^{\min}\quad\theta_2^{\min}\quad\theta_3^{\max}\right]^{\mathrm{T}},\ \Theta_8=\left[\theta_1^{\min}\quad\theta_2^{\min}\quad\theta_3^{\min}\right]^{\mathrm{T}}.$$

Based on different parameter-varying vector Θ_j (j = 1, 2, …, 8), Equation (11) can be rewritten as

$$\begin{aligned}A_{cj}(\Theta_j)&=A_{c0}+\sum_{i=1}^{3}\theta_i^{\dagger}A_{ci}\\ B_{c1j}(\Theta_j)&=B_{c10}+\sum_{i=1}^{3}\theta_i^{\dagger}B_{c1i}\\ B_{c2j}(\Theta_j)&=B_{c20}+\sum_{i=1}^{3}\theta_i^{\dagger}B_{c2i}\end{aligned}\tag{12}$$

where † denotes min or max.

Therefore, the polytopic model with eight vertices for the control system (10) can be expressed as

$$\begin{aligned}G_n(\Theta)&=\begin{bmatrix}A_c(\Theta)&B_{c1}(\Theta)&B_{c2}(\Theta)\\C_c&D_{c1}&D_{c2}\end{bmatrix}\\&=\sum_{j=1}^{8}\alpha_j\begin{bmatrix}A_{cj}(\Theta_j)&B_{c1j}(\Theta_j)&B_{c2j}(\Theta_j)\\C_c&D_{c1}&D_{c2}\end{bmatrix}\end{aligned}\tag{13}$$

where α_i denotes the weights of the eight vertices and the following condition should be followed.

$$\Theta=\sum_{j=1}^{8}\alpha_j\Theta_j,\quad \alpha_j\ge0,\quad \sum_{j=1}^{8}\alpha_j=1\quad(j=1,2,...,8)\tag{14}$$

α_i can be chosen to be the continuous function of Θ_j, which is related to the vertice value of Θ_j, the measured or estimated vehicle longitudinal velocity and tire cornering stiffness. For simplification, the weights of the eight vertices are given as (Jin *et al*., 2016)

$$\begin{aligned}&\alpha_1=abc,\ \ \alpha_2=ab(1-c),\ \ \alpha_3=a(1-b)c,\\&\alpha_4=(1-a)bc,\ \ \alpha_5=a(1-b)(1-c),\\&\alpha_6=(1-a)b(1-c),\ \ \alpha_7=(1-a)(1-b)c,\\&\alpha_8=(1-a)(1-b)(1-c)\end{aligned}\tag{15}$$

where

$$a=\frac{\theta_1-\theta_1^{\min}}{\theta_1^{\max}-\theta_1^{\min}},\quad b=\frac{\theta_2-\theta_2^{\min}}{\theta_2^{\max}-\theta_2^{\min}},\quad c=\frac{\theta_3-\theta_3^{\min}}{\theta_3^{\max}-\theta_3^{\min}}.$$

3. CONTROL SYSTEM DESIGN

3.1. Overall Control Framework

The path-tracking control system diagram of 4WIS-4WID EV is depicted in Figure 3. It can be seen from Figure 3 that the path-tracking control system mainly consists of two parts: (1) longitudinal motion control; (2) lateral and

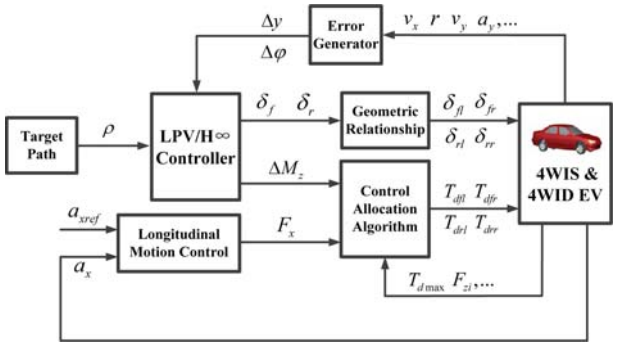

Figure 3. Path-tracking control system diagram of 4WIS-4WID EV.

yaw motion control. Longitudinal motion control aims to make the vehicle achieve ideal longitudinal motion response by the longitudinal force derived from in-wheel motors. The desired longitudinal force is directly calculated with the sum of four tire longitudinal forces. Considering that longitudinal motion control is not the emphasis of path-tracking control, this paper mainly focuses on the lateral and yaw motion control of 4WIS-4WID EV. Lateral and yaw motion control is realized by 4WS and DYC. The front and rear steering angle signals and the external yaw moment signal are calculated by the proposed LPV/H_∞ controller. Then, the steering angle of each wheel is figured out based on the Ackerman steering geometry using the front and rear steering angle signals of the single track model. The drive torque of each wheel is calculated based on the control allocation algorithm according to the external yaw moment signal of DYC and the desired longitudinal force of longitudinal motion control.

3.2. LPV/H_∞ Controller Design

For controller design, appropriate performance weighting functions are added to the control system G_n. The block diagram of the closed-loop control system is shown in Figure 4. K denotes the feedback controller. w denotes the external disturbance, which is described by the target path information. y represents the system output, which can be measured or observed. u is the control input of the system, which consists of δ_f, δ_r, and ΔM_z. Outputs z_1 and z_2 are used to evaluate the robust performance of the closed-loop system. Besides, weighting functions W_u and W_y represent the performance outputs of u and y, respectively.

To get good path-tracking performance and transient response, the performance weighting function W_y is selected, which is given by

$$W_y = \begin{bmatrix} \dfrac{0.12s^2+0.216s+1.2}{s^2+4s+0.01} & 0 \\ 0 & \dfrac{0.12s^2+0.216s+1.2}{s^2+8s+0.01} \end{bmatrix} \tag{16}$$

which indicates that the steady error requirements of Δy and $\Delta\varphi$ are both less than 1 %.

The performance weighting function W_u is selected based on the capability of actuators. The front and rear steering angles are limited to be less than 45 degrees and the maximum external yaw moment is set as 1000 N·m. Finally, W_u is defined as

$$W_u = \mathrm{diag}\left[1.273,\quad 1.273,\quad 0.001\right] \tag{17}$$

Furthermore, the weighting functions W_y and W_u can be rewritten in the state-space form.

$$\begin{aligned} \dot{x}_{w1} &= A_{w1}x_{w1} + B_{w1}u_{w1} \\ y_{w1} &= C_{w1}x_{w1} + D_{w1}u_{w1} \end{aligned} \tag{18}$$

$$\begin{aligned} \dot{x}_{w2} &= A_{w2}x_{w2} + B_{w2}u_{w2} \\ y_{w2} &= C_{w2}x_{w2} + D_{w2}u_{w2} \end{aligned} \tag{19}$$

Finally, the closed-loop control system can be simplified as a generalized system shown in Figure 5. The generalized system P can be expressed as

$$\begin{bmatrix} \dot{x} \\ z \\ y \end{bmatrix} = \begin{bmatrix} A(\Theta) & B_1(\Theta) & B_2(\Theta) \\ C_1 & D_{11} & D_{12} \\ C_2 & D_{21} & D_{22} \end{bmatrix} \begin{bmatrix} x \\ w \\ u \end{bmatrix} \tag{20}$$

where $x = \begin{bmatrix} x_c^{\mathrm{T}} & x_{w1}^{\mathrm{T}} & x_{w2}^{\mathrm{T}} \end{bmatrix}^{\mathrm{T}}$, $z = \begin{bmatrix} z_1^{\mathrm{T}} & z_2^{\mathrm{T}} \end{bmatrix}^{\mathrm{T}}$, $w = \dfrac{1}{\rho}$,

$u = \begin{bmatrix} \delta_f & \delta_r & \Delta M_z \end{bmatrix}^{\mathrm{T}}$, $A(\Theta) = \begin{bmatrix} A_c(\Theta) & 0 & 0 \\ B_{w1}C_c & A_{w1} & 0 \\ 0 & 0 & A_{w2} \end{bmatrix}$,

$B_1(\Theta) = \begin{bmatrix} B_{1c}(\Theta) \\ B_{w1}D_{c1} \\ 0 \end{bmatrix}$, $B_2(\Theta) = \begin{bmatrix} B_{2c}(\Theta) \\ B_{w1}D_{c2} \\ B_{w2} \end{bmatrix}$,

$C_1 = \begin{bmatrix} D_{w1}C_c & C_{w1} & 0 \\ 0 & 0 & C_{w2} \end{bmatrix}$, $D_{11} = \begin{bmatrix} D_{w1}D_{c1} \\ 0 \end{bmatrix}$,

$D_{12} = \begin{bmatrix} D_{w1}D_{c2} \\ D_{w2} \end{bmatrix}$, $C_2 = \begin{bmatrix} C_c & 0 & 0 \end{bmatrix}$, $D_{21} = D_{c1}$, $D_{22} = D_{c2}$.

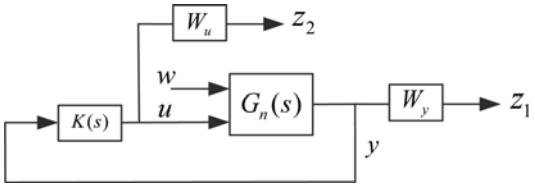

Figure 4. Block diagram of the closed-loop control system.

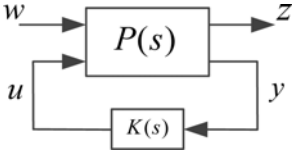

Figure 5. Generalized system.

As shown in Figure 5, a LPV/H_∞ controller $K(s)$ is designed for path tracking of the 4WIS-4WID EV, which can be written in the state-space form:

$$\begin{aligned}\dot{x}_{\mathrm{K}} &= A_{\mathrm{K}}(\Theta)x_{\mathrm{K}} + B_{\mathrm{K}}(\Theta)y\\ u &= C_{\mathrm{K}}(\Theta)x_{\mathrm{K}} + D_{\mathrm{K}}(\Theta)y\end{aligned} \tag{21}$$

where x_{K} denotes the state vector of controller, A_{K}, B_{K}, C_{K} and D_{K} are the controller parametric matrices needed to solve.

Applying the controller (21) to the LPV system (20) yields the following closed-loop system.

$$\begin{aligned}\dot{\xi} &= A_{\mathrm{cl}}(\Theta)\xi + B_{\mathrm{cl}}(\Theta)w\\ z &= C_{\mathrm{cl}}\xi + D_{\mathrm{cl}}w\end{aligned} \tag{22}$$

where $\xi = \begin{bmatrix} x \\ x_{\mathrm{K}} \end{bmatrix}$, $A_{\mathrm{cl}}(\Theta) = \begin{bmatrix} A + B_2 D_{\mathrm{K}} C_2 & B_2 C_{\mathrm{K}} \\ B_{\mathrm{K}} C_2 & A_{\mathrm{K}} \end{bmatrix}$,

$B_{\mathrm{cl}}(\Theta) = \begin{bmatrix} B_1 \\ 0 \end{bmatrix}$, $C_{\mathrm{cl}} = \begin{bmatrix} C_1 & 0 \end{bmatrix}$, $D_{\mathrm{cl}} = D_{11}$.

The aforementioned matrices A, B_1, B_2, A_{cl}, B_{cl}, A_{K}, B_{K}, C_{K} and D_{K} are all related to the parameter-varying vector Θ. As to the polytopic model, these matrices at the jth vertice can be expressed as A_{j}, $B_{1\mathrm{j}}$, $B_{2\mathrm{j}}$, A_{clj}, B_{clj}, A_{Kj}, B_{Kj}, C_{Kj} and D_{Kj}.

The designed LPV/H_∞ controller should make the closed-loop system (22) asymptotically stable, and the infinite norm of the transfer function from the external disturbance w to the measurement output z should less than 1, namely, $\|T_{\mathrm{wz}}(s)\|_\infty < 1$. We first introduce the following lemma.

Lemma 1 (Yang *et al*., 2008). Given the positive constant γ, considering the closed-loop system (22) at the jth vertice, the following two conditions are equivalent.

(1) The closed-loop system is asymptotically stable and the energy to energy gain satisfies

$$\Gamma_{\mathrm{ee}} < \gamma \tag{23}$$

(2) There exists a symmetric positive definite matrix X_{clj} satisfying the following condition:

$$\begin{bmatrix} A_{\mathrm{clj}}^{\mathrm{T}} X_{\mathrm{clj}} + X_{\mathrm{clj}} A_{\mathrm{clj}} & X_{\mathrm{clj}} B_{\mathrm{clj}} & C_{\mathrm{cl}}^{\mathrm{T}} \\ B_{\mathrm{clj}}^{\mathrm{T}} X_{\mathrm{clj}} & -\gamma I & D_{\mathrm{cl}}^{\mathrm{T}} \\ C_{\mathrm{cl}} & D_{\mathrm{cl}} & -\gamma I \end{bmatrix} < 0 \tag{24}$$

As to the matrix X_{clj}, if $X_{\mathrm{clj}} \in \mathbb{R}^{\mathrm{n}\times\mathrm{n}}$ and $X_{\mathrm{clj}} = X_{\mathrm{clj}}^{\mathrm{T}}$, for the arbitray matrix $0 \neq A_{\mathrm{p}} \in \mathbb{R}^{\mathrm{n}}$, there exists $A_{\mathrm{p}}^{\mathrm{T}} X_{\mathrm{clj}} A_{\mathrm{p}} > 0$, the matrix X_{clj} can be regarded as a symmetric positive definite matrix.

Based on the aforementioned lemma, we introduce the following theorem to solve the LPV/ H_∞ controller.

Theorem 1. Given the positive constant γ, a sub-optimal output-feedback controller exists if and only if there exists symmetric positive definite matrices X_{j} and Y_{j} and matrices $\hat{A}_{\mathrm{j}}$, $\hat{B}_{\mathrm{j}}$, $\hat{C}_{\mathrm{j}}$ and $\hat{D}_{\mathrm{j}}$ satisfying the following conditions:

$$\begin{bmatrix} A_{\mathrm{j}}X_{\mathrm{j}} + X_{\mathrm{j}}A_{\mathrm{j}}^{\mathrm{T}} + B_{2\mathrm{j}}\hat{C}_{\mathrm{j}} + (B_{2\mathrm{j}}\hat{C}_{\mathrm{j}})^{\mathrm{T}} & \hat{A}_{\mathrm{j}}^{\mathrm{T}} + (A_{\mathrm{j}} + B_{2\mathrm{j}}\hat{D}_{\mathrm{j}}C_2) \\ * & A_{\mathrm{j}}^{\mathrm{T}}Y_{\mathrm{j}} + Y_{\mathrm{j}}A_{\mathrm{j}} + \hat{B}_{\mathrm{j}}C_2 + (\hat{B}_{\mathrm{j}}C_2)^{\mathrm{T}} \\ * & * \\ * & * \end{bmatrix}$$
$$\begin{bmatrix} B_{1\mathrm{j}} & (C_1 X_{\mathrm{j}})^{\mathrm{T}} \\ Y_{\mathrm{j}}B_{1\mathrm{j}} & C_1^{\mathrm{T}} \\ -\gamma I & D_{11}^{\mathrm{T}} \\ * & -\gamma I \end{bmatrix} < 0 \tag{25}$$

$$\begin{bmatrix} X_{\mathrm{j}} & I \\ I & Y_{\mathrm{j}} \end{bmatrix} > 0 \tag{26}$$

where $*$ denotes the terms that can be obtained by symmetry.

Proof. Since the matrix variable X_{clj} and the controller parameter matrices A_{Kj}, B_{Kj}, C_{Kj} and D_{Kj} in Equation (24) are strongly nonlinear, it is difficult to obtain the output-feedback controller by solving Equation (24). Based on the variable substitution method, Equation (24) can be transformed into the standard form of linear matrix inequality (LMI), which is easy to solve by LMI Toolbox. In the variable substitution method, a set of new matrix variables are proposed. Then, the original nonlinear matrix inequality is transformed into LMI with the new matrix variables. Thus, the results of the new matrix variables can be figured out using the LMI approach. Based on the substitution relationship between the new and original matrix variables, the results of the original matrix variables are easy to work out.

According to the Lemma 1, the matrix variable X_{clj} and its inverse matrix are partitioned as

$$X_{\mathrm{clj}} = \begin{bmatrix} Y_{\mathrm{j}} & N_{\mathrm{j}} \\ N_{\mathrm{j}}^{\mathrm{T}} & W_{\mathrm{j}} \end{bmatrix}, \quad X_{\mathrm{clj}}^{-1} = \begin{bmatrix} X_{\mathrm{j}} & M_{\mathrm{j}} \\ M_{\mathrm{j}}^{\mathrm{T}} & Z_{\mathrm{j}} \end{bmatrix} \tag{27}$$

where X_{j} and Y_{j} are symmetric positive definite matrices. Based on the equation $X_{\mathrm{clj}}X_{\mathrm{clj}}^{-1} = I$, it yields

$$X_{\mathrm{clj}} \begin{bmatrix} X_{\mathrm{j}} \\ M_{\mathrm{j}}^{\mathrm{T}} \end{bmatrix} = \begin{bmatrix} I \\ 0 \end{bmatrix} \tag{28}$$

Furthermore, we have

$$X_{\mathrm{clj}} \begin{bmatrix} X_{\mathrm{j}} & I \\ M_{\mathrm{j}}^{\mathrm{T}} & 0 \end{bmatrix} = \begin{bmatrix} I & Y_{\mathrm{j}} \\ 0 & N_{\mathrm{j}}^{\mathrm{T}} \end{bmatrix} \tag{29}$$

Defining two matrices

$$F_{1\mathrm{j}} = \begin{bmatrix} X_{\mathrm{j}} & I \\ M_{\mathrm{j}}^{\mathrm{T}} & 0 \end{bmatrix}, \quad F_{2\mathrm{j}} = \begin{bmatrix} I & Y_{\mathrm{j}} \\ 0 & N_{\mathrm{j}}^{\mathrm{T}} \end{bmatrix} \tag{30}$$

Then, Equation (29) can be rewritten as $X_{\mathrm{clj}}F_{1\mathrm{j}} = F_{2\mathrm{j}}$. Based on this equation, the following equations can be derived.

$$F_{1j}^{T}X_{clj}A_{clj}F_{1j} = F_{2j}^{T}A_{clj}F_{1j} = \begin{bmatrix} A_jX_j + B_{2j}(D_{Kj}C_2X_j + C_{Kj}M_j^{T}) \\ Y_j(A_j + B_{2j}D_{Kj}C_2)X_j + N_jB_{Kj}C_2X_j + Y_jB_{2j}C_{Kj}M_j^{T} + N_jA_{Kj}M_j^{T} \\ A_j + B_{2j}D_{Kj}C_2 \\ Y_jA_j + (Y_jB_{2j}D_{Kj} + N_jB_{Kj})C_2 \end{bmatrix} \quad (31)$$

$$F_{1j}^{T}X_{clj}B_{clj} = \begin{bmatrix} B_{1j} \\ Y_jB_{1j} \end{bmatrix} \quad (32)$$

$$C_{cl}F_{lj} = \begin{bmatrix} C_1X_j & C_1 \end{bmatrix} \quad (33)$$

$$F_{1j}^{T}X_{clj}F_{1j} = F_{2j}^{T}F_{1j} = \begin{bmatrix} X_j & I \\ I & Y_j \end{bmatrix} \quad (34)$$

To transform Equation (24) into the standard form of LMI, based on the aforementioned equations, the following new matrix variables are defined for variable substitution.

$$\begin{aligned} \hat{A}_j &= Y_j(A_j + B_{2j}D_{Kj}C_2)X_j \\ &\quad + N_jB_{Kj}C_2X_j + Y_jB_{2j}C_{Kj}M_j^{T} + N_jA_{Kj}M_j^{T} \\ \hat{B}_j &= Y_jB_{2j}D_{Kj} + N_jB_{Kj} \\ \hat{C}_j &= D_{Kj}C_2X_j + C_{Kj}M_j^{T} \\ \hat{D}_j &= D_{Kj} \end{aligned} \quad (35)$$

From Equation (35), it can be seen that the controller parameter matrices A_{Kj}, B_{Kj}, C_{Kj} and D_{Kj} are the unique solution with the given symmetric positive definite matrices X_j and Y_j and the full rank matrices M_j and N_j.

By pre-multiplying diag$\{F_{1j}^{T}, I, I\}$ and post-multiplying diag$\{F_{1j}, I, I\}$ on both sides of Equation (24) respectively and combining the Equations (31) to (35), we can readily obtain the equivalent condition Equation (25). We can see that it is a standard LMI about the matrix variables $\hat{A}_j$, $\hat{B}_j$, $\hat{C}_j$, $\hat{D}_j$, X_j and Y_j. So the solving method of LMI is the same with Equation (25).

After obtaining a feasible solution of Equation (25), to find the controller parameter matrices A_{Kj}, B_{Kj}, C_{Kj} and D_{Kj} according to the substitution relationship in Equation (35), the results of matrices M_j and N_j must be worked out firstly.

Based on the identity $X_{clj}^{-1}X_{clj} = I$, it follows that

$$M_jN_j^{T} = I - X_jY_j \quad (36)$$

After getting the values of matrices X_j and Y_j, the results of matrices M_j and N_j can be obtained by the singular value decomposition of $I - X_jY_j$. Since X_{cl} is a symmetric positive definite matrix, the condition in Equation (26) can be derived. Therefore, $I - X_jY_j > 0$. In general, it can be concluded that the matrices M_j and N_j can always be obtained by the singular value decomposition to satisfy Equation (25).

Finally, the controller parameter matrices A_{Kj}, B_{Kj}, C_{Kj} and D_{Kj} are derived as follows and this finishes the proof.

$$\begin{aligned} A_{Kj} &= N_j^{-1}[\hat{A}_j - X_j(A_j - B_{2j}D_{Kj}C_2)Y_j \\ &\quad - \hat{B}_jC_2Y_j - X_jB_{2j}\hat{C}_j](M_j^{T})^{-1} \\ B_{Kj} &= N_j^{-1}(\hat{B}_j - Y_jB_{2j}D_{Kj}) \\ C_{Kj} &= (\hat{C}_j - D_{Kj}C_2X_j)(M_j^{T})^{-1} \\ D_{Kj} &= \hat{D}_j \end{aligned} \quad (37)$$

Based on Equations (25), (26) and (37), eight vertice controllers $K_j(s)$ ($j = 1, 2, \ldots, 8$) can be figured out. Finally, the output-feedback LPV/H_∞ controller $K(s)$ can be expressed as

$$\begin{bmatrix} A_K & B_K \\ C_K & D_K \end{bmatrix} = \sum_{j=1}^{8}\alpha_j \begin{bmatrix} A_{Kj} & B_{Kj} \\ C_{Kj} & D_{Kj} \end{bmatrix} \quad (38)$$

3.3. Control Allocation Algorithm

Since 4WIS-4WID EV is an over-actuated system, the torque of each in-wheel motor can be different to make the vehicle obtain better dynamic performance. The external yaw moment ΔM_z can be generated by the torque allocation between the left and right side wheels to improve vehicle handling stability. The torque allocation between the front and rear wheels can be in favor of vehicle power performance and economy property. In this section, the control allocation algorithm is proposed to improve vehicle handling stability.

The wheel steering angle is normally very small at high vehicle speed, so the effect of steering angles on total longitudinal force and external yaw moment can be ignored. The external yaw moment ΔM_z is expressed in Equation (2), and the total longitudinal force can be written as

$$F_x = F_{xfl} + F_{xfr} + F_{xrl} + F_{xrr} \quad (39)$$

Providing that each tire works in the steady state and the rolling resistance is neglected, each tire longitudinal force can be expressed as

$$F_{xi} = \frac{T_{di}}{R_w}, \quad (i = fl, fr, rl, rr) \quad (40)$$

where T_{di} denotes the torque of each in-wheel motor and R_w denotes the tire rolling radius.

Substitution of Equation (40) into Equations (2) and (39) yields that

$$V = B_xU \quad (41)$$

where $U = [T_{dfl}\ T_{dfr}\ T_{drl}\ T_{drr}]^{T}$, $V = [F_x\ \Delta M_z]^{T}$ and B_x is the effectiveness matrix, which is written as

$$B_x = \begin{bmatrix} \frac{1}{R_w} & \frac{1}{R_w} & \frac{1}{R_w} & \frac{1}{R_w} \\ -\frac{B}{2R_w} & \frac{B}{2R_w} & -\frac{B}{2R_w} & \frac{B}{2R_w} \end{bmatrix}.$$

For control allocation, one objective is to minimize the allocation error:

$$\begin{aligned} &\min \left\| W_{\mathrm{V}}(B_{\mathrm{x}}U - V) \right\| \\ &\text{s.t. } U^{-} \le U \le U^{+} \end{aligned} \tag{42}$$

where W_{V} is the weighting matrix of generalized force, U^{-} and U^{+} are the lower and upper bounds of control vector U, respectively.

From Equation (42), it can be seen that the control allocation problem should be solved in the constraint range. The constraints of actuators include the capability constraint of actuators and the constraint of road conditions, which are given by

$$\begin{aligned} &T_{\mathrm{d\,min}} \le T_{\mathrm{di}} \le T_{\mathrm{d\,max}} \\ &\left| T_{\mathrm{di}} \right| \le \mu F_{\mathrm{zi}} R_{\mathrm{w}}, \quad (i = fl, fr, rl, rr) \end{aligned} \tag{43}$$

where F_{zi} denotes the vertical load of each tire. $T_{\mathrm{d\,min}}$ and $T_{\mathrm{d\,max}}$ denote the minimal and maximal output torques of the in-wheel motor, respectively. The output torque of the in-wheel motor is related to the working speed, and the relationship is illustrated in Figure 6. From the figure, we can see that the motor works in the constant torque region at the speed lower than the base speed. When the motor's speed is higher than the base speed, the output torque decreases with the increase of speed. As a result, the motor works in the constant power region.

Furthermore, another optimization objective can be expressed as

$$\begin{aligned} &\min \left\| W_{\mathrm{U}}(U - U_{\mathrm{d}}) \right\| \\ &\text{s.t. } U^{-} \le U \le U^{+} \end{aligned} \tag{44}$$

where U_{d} is the target control value, W_{U} is the weighting matrix of actuators.

Combining the Equations (42) and (44), the control allocation algorithm can be expressed as

$$\begin{aligned} &U = \arg\min_{\mathrm{U}\in\Xi} \left\| W_{\mathrm{U}}(U - U_{\mathrm{d}}) \right\|_2 \\ &\Xi = \arg\min_{U^{-} \le U \le U^{+}} \left\| W_{\mathrm{V}}(B_{\mathrm{x}}U - V) \right\|_2 \end{aligned} \tag{45}$$

The above allocation method is also called the sequential least square (SLS) allocation algorithm. The first step is to figure out the control vector set Ξ to minimize the weighted allocation error $\left\| W_{\mathrm{V}}(B_{\mathrm{x}}U - V) \right\|_2$ in the feasible region. Then, a desired control vector U is selected, which is the closest to target control value U_{d}.

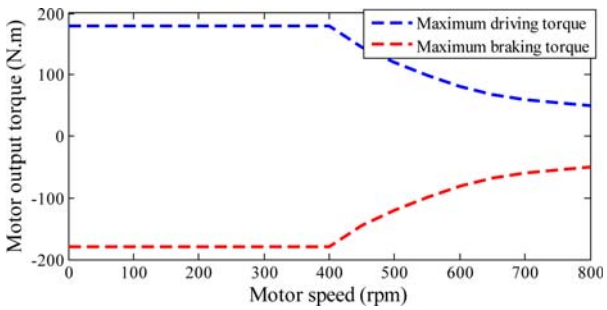

Figure 6. Maximum output torque of the in-wheel motor.

For convenience, the aforementioned two steps can be combined into only one step by weighting parameter λ using weighted least square (WLS) allocation algorithm, which can be expressed as

$$\begin{aligned} &\min J = \lambda \left\| W_{\mathrm{V}}(B_{\mathrm{x}}U - V) \right\|_2^2 + \left\| W_{\mathrm{U}}(U - U_{\mathrm{d}}) \right\|_2^2 \\ &\text{s.t. } U^{-} \le U \le U^{+} \end{aligned} \tag{46}$$

Compared with SLS allocation algorithm, the computing time of WLS allocation algorithm can be greatly reduced, and λ is usually set very large so as to minimize the allocation error.

Furthermore, the objective function in Equation (46) can be simplified as

$$J = \left\| \underbrace{\begin{pmatrix} \lambda^{\frac{1}{2}} W_{\mathrm{V}} B_{\mathrm{x}} \\ W_{\mathrm{U}} \end{pmatrix}}_{\mathrm{A_x}} U - \underbrace{\begin{pmatrix} \lambda^{\frac{1}{2}} W_{\mathrm{U}} V \\ W_{\mathrm{U}} U_{\mathrm{d}} \end{pmatrix}}_{\mathrm{b_x}} \right\|_2^2 \tag{47}$$

In general, the control allocation problem using WLS allocation algorithm can be written as

$$\begin{aligned} &\min \left\| A_{\mathrm{x}}U - b_{\mathrm{x}} \right\|_2^2 \\ &\text{s.t. } U^{-} \le U \le U^{+} \end{aligned} \tag{48}$$

Since the working output torque of each in-wheel motor is proportional to the vertical load of corresponding tire, the weighting matrix of actuators W_{U} is defined as

$$W_{\mathrm{U}} = \mathrm{diag}\left[\frac{1}{F_{\mathrm{zfl}}}, \quad \frac{1}{F_{\mathrm{zfr}}}, \quad \frac{1}{F_{\mathrm{zrl}}}, \quad \frac{1}{F_{\mathrm{zrr}}} \right] \tag{49}$$

The weighting matrix of generalized force W_{V} is used to adjust the priority of the total longitudinal force and external yaw moment, i.e. the weight of external yaw moment can be increased to improve the handling stability of vehicle when the vehicle is driven in the condition of large lateral acceleration. Since the 4WS technique has been adopted to improve the dynamic performance of vehicle, the weights of the total longitudinal force and external yaw moment are set as the same value temporarily.

$$W_{\mathrm{V}} = \mathrm{diag}\left[1, \quad 1 \right] \tag{50}$$

4. SIMULATIONS AND EVALUATIONS

To evaluate the designed LPV/H_∞ controller for path tracking of the 4WIS-4WID EV, two simulation cases are conducted based on a high-fidelity, full-vehicle model constructed in CarSim. The vehicle parameters in the simulation are listed in Table 1 and the prototype vehicle is

Table 1. Vehicle parameters in the simulation.

Parameter	Symbol	Unit	Value
Vehicle mass	m	kg	648
Vehicle yaw inertia	I_z	kg·m^2	262
Front wheel base	l_f	m	0.957
Rear wheel base	l_r	m	0.577
Wheelbase	l	m	1.534
Track	B	m	0.97
Front tire cornering stiffness	k_{f0}	N/rad	15000
Rear tire cornering stiffness	k_{r0}	N/rad	18000

Figure 7. Prototype vehicle of the 4WIS-4WID EV.

depicted in Figure 7.

4.1. Single Lane-changing Maneuver

In this simulation case, a single-lane change maneuver for path tracking of the 4WIS-4WID EV is carried out based on the designed LPV/H_∞ controller and control allocation algorithm. To better show the performance of the LPV/H_∞ controller, the path-tracking performance of the fixed gain H_∞ controller is shown in the simulation results as well. In the simulation case, the vehicle longitudinal velocity is set as 20 m/s, and the road friction coefficient is set as 0.3.

The path-tracking results of the two controllers in the single lane-changing maneuver are plotted in Figure 8. To better show the path-tracking performance, the lateral position errors and yaw angle errors are displayed in

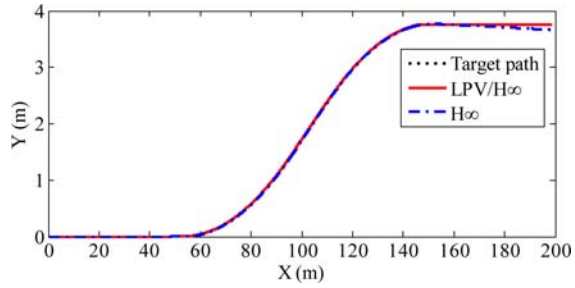

Figure 8. Path-tracking results in the single lane-changing simulation.

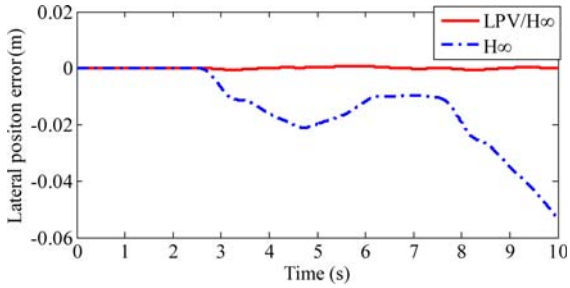

Figure 9. Lateral position errors in the single lane-changing simulation.

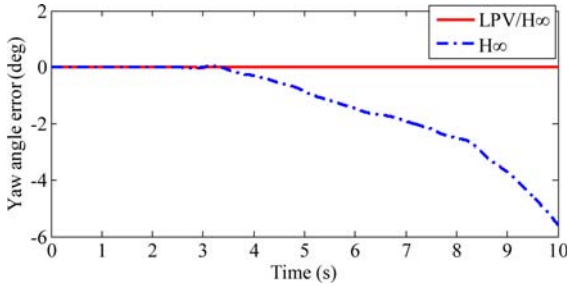

Figure 10. Yaw angle errors in the single lane-changing simulation.

Figures 9 and 10, respectively. It can be easily observed that both the lateral position error and yaw angle error of the LPV/H_∞ controller are much smaller than that of fixed gain H_∞ controller, which indicates that the designed LPV/H_∞ controller has a better path-tracking performance. Moreover, the tracking error of the fixed gain H_∞ controller cannot converge to zero, which tends to be unstable.

The variations of front and rear steering angles and external yaw moment are illustrated in Figures 11 ~ 13, from which we can see that both of the front and rear steering angles of the fixed gain H_∞ controller are much larger than that of LPV/H_∞ controller. The outputs of fixed gain H_∞ controller cannot converge to the steady state values, but it has the opposite conclusion for LPV/H_∞ controller. It can be inferred that fixed gain H_∞ controller makes full use of larger steering angles and external yaw

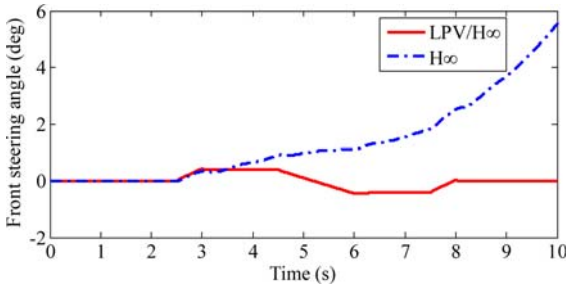

Figure 11. Front steering angles in the single lane-changing simulation.

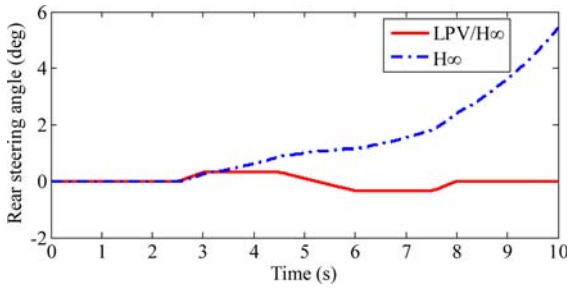

Figure 12. Rear steering angles in the single lane-changing simulation.

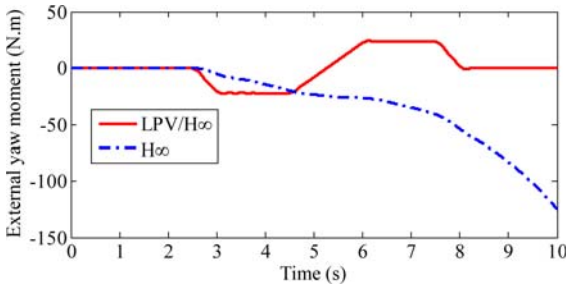

Figure 13. External yaw moments in the single lane-changing simulation.

moment to improve the vehicle dynamic performance. However, the vehicle tends to be unstable. The results prove that LPV/H_∞ controller has better control effect when vehicle runs on a low adhesion road. The lateral velocities of two controllers are illustrated in Figure 14, and it can be

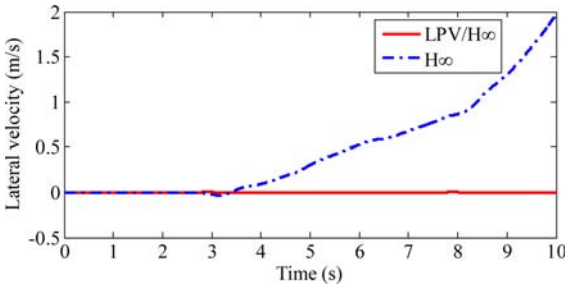

Figure 14. Lateral velocities in the single lane-changing simulation.

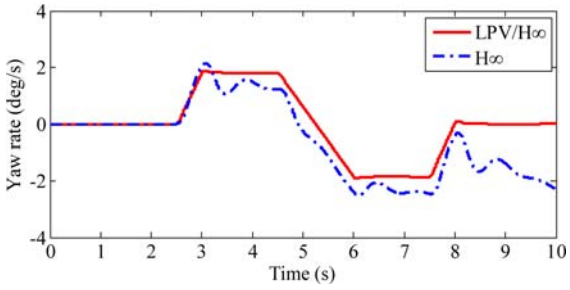

Figure 15. Yaw rates in the single lane-changing simulation.

observed that LPV/H_∞ controller helps the vehicle obtain smaller lateral velocity, which is nearly close to zero. Namely, the vehicle with LPV/H_∞ controller has better handling stability. Besides, the yaw rates are displayed in Figure 15.

4.2. Circular Path Maneuver

In the circular path maneuver, it aims to verify the superiority of 4WS+DYC control system, which is compared with AFS, AFS+DYC, 4WS and 4WS+DYC. The vehicle with a constant speed of 20 m/s suddenly enters a circular path of 115 m radius with the road friction coefficient of 0.8. It is worth mentioning that the path-tracking controllers of four control systems all use the LPV/H_∞ controllers.

Figure 16 shows the path-tracking results of four control systems in the circular path simulation case, and it can be obviously seen that AFS has the largest tracking error. Furthermore, the lateral position errors and yaw angle

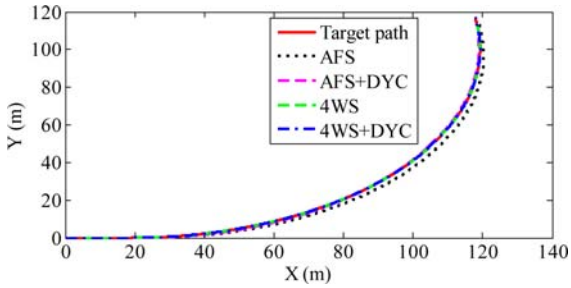

Figure 16. Path-tracking results in the circular path simulation.

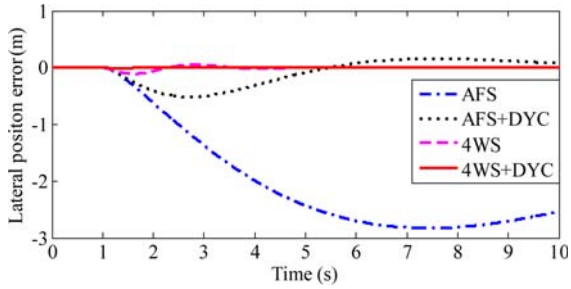

Figure 17. Lateral position errors in the circular path simulation.

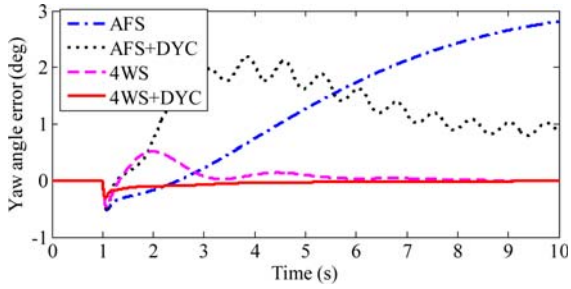

Figure 18. Yaw angle errors in the circular path simulation.

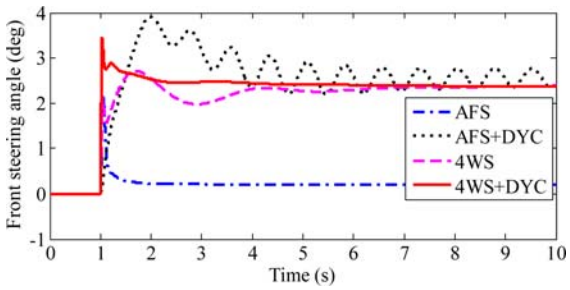

Figure 19. Front steering angles in the circular path simulation.

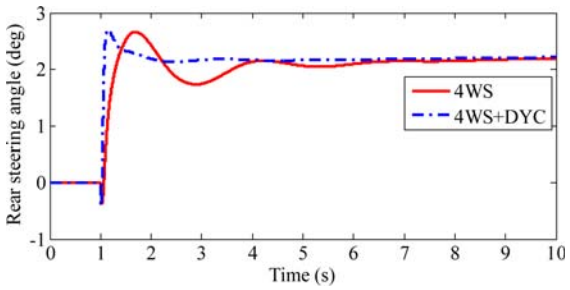

Figure 20. Rear steering angles in the circular path simulation.

errors are plotted in Figures 17 and 18, respectively. It can be found from the figures that 4WS+DYC has the smallest lateral position error and yaw angle error and the highest convergence rate, which implies 4WS+DYC has the best path-tracking performance among the four control systems.

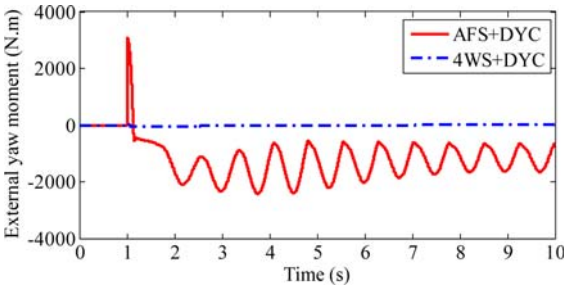

Figure 21. External yaw moments in the circular path simulation.

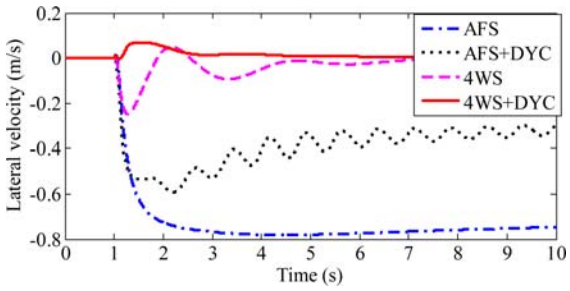

Figure 22. Lateral velocities in the circular path simulation.

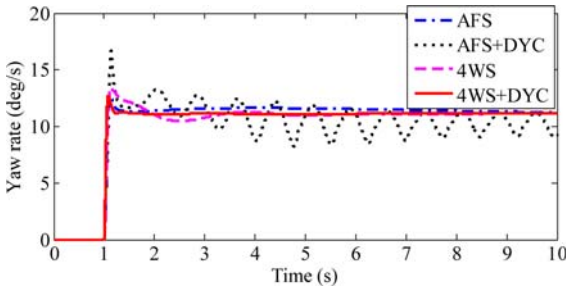

Figure 23. Yaw rates in the circular path simulation.

Besides, it can be seen that the path-tracking performance of 4WS is better than that of AFS+DYC, which owes to the steering ability of the rear wheels on 4WS system to reduce the sideslip angle of the vehicle effectively and then decrease the path-tracking errors. The simulation results of control variables front and rear steering angles and external yaw moment are illustrated in Figures 19 ~ 21. Figure 22 illustrates the variations of lateral velocities, from which it can be seen that 4WS+DYC can make the lateral velocity fast coverage to zero. In contrast, AFS and AFS+DYC have bigger lateral velocities, which can deteriorate the handling stability of the vehicle, and 4WS has slower convergence rate. Moreover, the yaw rates are depicted in Figure 23 in detail.

5. CONCLUSION

In this paper, a path-tracking control method for a 4WIS-4WID EV is presented. The path-tracking mathematical model is derived based on the lateral position error and yaw angle error which are the performance indexes to evaluate the designed controllers. To suppress the effect of the uncertainties of vehicle model, the path-tracking model is transformed into a polytopic model with eight vertices utilizing LPV method. Based on LMI approach, the high-level LPV/H_∞ controller is designed for path tracking of the 4WIS-4WID EV. The lower-level controller is designed for torque allocation between the left and right side wheels to generate desired total longitudinal force and external yaw moment. Numerical simulations are carried out to assess the effectiveness of the designed controllers and to compare the performance of different control systems, i.e. AFS, AFS+DYC, 4WS and 4WS+DYC based on a high-fidelity, full-vehicle model constructed in CarSim. Simulation results show that the LPV/H_∞ controller has larger control potential on low adhesion coefficient road compared with the fixed gain H_∞ controller. 4WS+DYC control system has better path-tracking performance and handling stability. Experimental validation of the proposed path-tracking control method will be carried out in the future.

ACKNOWLEDGEMENT–This study is supported by National Key R&D Program of China (Grant No. 2018YFB0104802) and

National Nature Science Foundation of China (U1564207). The authors would like to express their sincere thanks to them for providing research funding.

REFERENCES

Backfrieder, C., Ostermayer, G. and Mecklenbräuker, C. F. (2017). Increased traffic flow through node-based bottleneck prediction and V2X communication. *IEEE Trans. Intelligent Transportation Systems* **18**, **2**, 349–363.

Chen, S., Shu, J. and Yang, L. (2006). Research on vehicle control technology using four-wheel independent steering system. *J. Beijing Institute of Technology* **15**, **1**, 22–26.

El Hajjaji, E. and Bentalba, S. (2003). Fuzzy path tracking control for automatic steering of vehicles. *Robotics and Autonomous Systems* **43**, **4**, 203–213.

Goodarzi, A., Sabooteh, A. and Esmailzadeh, E. (2008). Automatic path control based on integrated steering and external yaw-moment control. *Proc. Institution of Mechanical Engineers, Part K: J. Multi-body Dynamics* **222**, **2**, 189–200.

Guo, J., Hu, P., Li, L. and Wang, R. (2012). Design of automatic steering controller for trajectory tracking of unmanned vehicles using genetic algorithms. *IEEE Trans. Vehicular Technology* **61**, **7**, 2913–2924.

Hang, P., Chen, X., Luo, F. and Fang, S. (2017a). Robust control of a four-wheel-independent-steering electric vehicle for path tracking. *SAE Int. J. Vehicle Dynamics, Stability, and NVH* **1**, **2**, 307–316.

Hang, P., Chen, X., Fang, S. and Luo, F. (2017b). Robust control for four-wheel-independent-steering electric vehicle with steer-by-wire system. *Int. J. Automotive Technology* **18**, **5**, 785–797.

Hang, P., Luo, F., Fang, S. and Chen, X. (2017c). Path tracking control of a four-wheel-independent-steering electric vehicle based on model predictive control. *Proc. IEEE 36th Chinese Control Conf. (CCC)*, 9360–9366.

Hiraoka, T., Nishihara, O. and Kumamoto, H. (2009). Automatic path-tracking controller of a four-wheel steering vehicle. *Vehicle System Dynamics: Int. J. Vehicle Mechanics and Mobility* **47**, **10**, 1205–1227.

Hu, C., Wang, R., Yan, F. and Chen, N. (2015). Should the desired heading in path following of autonomous vehicles be the tangent direction of the desired path. *IEEE Trans. Intelligent Transportation Systems* **16**, **6**, 3084–3094.

Hu, C., Wang, R., Yan, F. and Chen, N. (2016). Output constraint control on path following of four-wheel independently actuated autonomous ground vehicles. *IEEE Trans. Vehicular Technology* **65**, **6**, 4033–4043.

Janbakhsh, A. A., Khaknejad, M. B. and Kazemi, R. (2013). Simultaneous vehicle-handling and path-tracking improvement using adaptive dynamic surface control via a steer-by-wire system. *Proc. Institution of Mechanical Engineers, Part D: J. Automobile Engineering* **227**, **3**, 345–360.

Jin, X., Yin, G., Bian, C., Chen, J., Li, P. and Chen, N. (2016). Gain-scheduled vehicle handling stability control via integration of active front steering and suspension systems. *J. Dynamic Systems, Measurement, and Control* **138**, **1**, 014501-1–014501-12.

Kim, E., Kim, J. and Sunwoo, M. (2014). Model predictive control strategy for smooth path tracking of autonomous vehicles with steering actuator dynamics. *Int. J. Automotive Technology* **15**, **7**, 1155–1164.

Kobayashi, T., Katsuyama, E., Sugiura, H., Ono, E. and Yamamoto, M. (2017). Direct yaw moment control and power consumption of in-wheel motor vehicle in steady-state turning. *Vehicle System Dynamics: Int. J. Vehicle Mechanics and Mobility* **55**, **1**, 104–120.

Lam, T. L., Qian, H. and Xu, Y. (2010). Omnidirectional steering interface and control for a four-wheel independent steering vehicle. *IEEE/ASME Trans. Mechatronics* **15**, **3**, 329–338.

Mashadi, B., Ahmadizadeh, P. and Majidi, M. (2011). Integrated controller design for path following in autonomous vehicles. *SAE Paper No*. 2011-01-1032.

Mashadi, B., Ahmadizadeh, P., Majidi, M. and Mahmoodi-Kaleybar, M. (2015). Integrated robust controller for vehicle path following. *Multibody System Dynamics* **33**, **2**, 207–228.

Tchenderli-Braham, S. A., Hamerlain, F. and Saadia, N. (2015). Experimentations on the adaptive sliding mode control for a trajectory tracking applied on a bi-steerable car. *Int. J. Vehicle Design* **69**, **1-4**, 285–303.

Wang, H., Wang, D. and Peng, Z. H. (2015a). Adaptive neural control for cooperative path following of marine surface vehicles: state and output feedback. *Int. J. Systems Science* **47**, **2**, 343–359.

Wang, R., Chen, Y., Feng, D., Huang, X. and Wang, J. (2011). Development and performance characterization of an electric ground vehicle with independently actuated in-wheel motors. *J. Power Sources* **196**, **8**, 3962–3971.

Wang, R., Zhang, H., Wang, J., Yan, F. and Chen, N. (2015b). Robust lateral motion control of four-wheel independently actuated electric vehicles with tire force saturation consideration. *J. Franklin Institute* **352**, **2**, 645–668.

Xiong, L., Yu, Z., Wang, Y., Chen, Y. and Men, Y. (2012). Vehicle dynamics control of four in-wheel motor drive electric vehicle using gain scheduling based on tyre cornering stiffness estimation. *Vehicle System Dynamics: Int. J. Vehicle Mechanics and Mobility* **50**, **6**, 831–846.

Yakub, F., Abu, A., Sarip, S. and Mori, Y. (2016). Study of model predictive control for path-following autonomous ground vehicle control under crosswind effect. *J. Control Science and Engineering*, **2016**, 1–18.

Yakub, F. and Mori, Y. (2015). Comparative study of

autonomous path-following vehicle control via model predictive control and linear quadratic control. *Proc. Institution of Mechanical Engineers, Part D: J. Automobile Engineering* **229**, **12**, 1695–1714.

Yang, X., Wang, Z. and Peng, W. (2008). LPV model based robust gain scheduling control of vehicle stability. *SAE Paper No*. 2008-01-2598.

Yin, G., Wang, R. and Wang, J. (2015). Robust control for four wheel independently-actuated electric ground vehicles by external yaw-moment generation. *Int. J. Automotive Technology* **16**, **5**, 839–847.

You, S.-S. and Jeong, S.-K. (2002). Controller design and analysis for automatic steering of passenger cars. *Mechatronics* **12**, **3**, 427–446.

Yu, H., Duan, J., Taheri, S. and Cheng, H. (2015). A model predictive control approach combined unscented Kalman filter vehicle state estimation in intelligent vehicle trajectory tracking. *Advances in Mechanical Engineering* **7**, **5**, 1–14.

Zhang, H., Zhang, X. and Wang, J. (2014). Robust gain-scheduling energy-to-peak control of vehicle lateral dynamics stabilization. *Vehicle System Dynamics: Int. J. Vehicle Mechanics and Mobility* **52**, **3**, 309–340.

Zhao, H., Gao, B., Ren, B. and Chen, H. (2015). Integrated control of in-wheel motor electric vehicles using a triple-step nonlinear method. *J. Franklin Institute* **352**, **2**, 519–540.

Zhou, Y., Dey, K. C., Chowdhury, M. and Wang, K. C. (2017). Process for evaluating the data transfer performance of wireless traffic sensors for real-time intelligent transportation systems applications. *IET Intelligent Transport Systems* **11**, **1**, 18–27.

Zong, C., Liu, J., Zheng, H., Song, P. and Zhang, Q. (2011). Modeling and special conditions simulation of electric vehicle with 4WID/4WIS. *Qiche Gongcheng* **33**, **10**, 829–833.